Three-dimensional flux states as a model for the pseudogap phase of transition metal oxides

D. F. Schroeter* and S. Doniach
Department of Physics, Stanford University, Stanford, California 94305
(Received 8 January 2002; published 26 August 2002)

We propose that the pseudogap state observed in the transition metal oxides can be explained by a three-dimensional flux state, which exhibits spontaneously generated currents in its ground state due to electron-electron correlations. We compare the energy of the flux state to other classes of mean field states, and find that it is stabilized over a wide range of t and δ. The signature of the state will be peaks in the neutron diffraction spectra, the location and intensity of which are presented. The dependence of the pseudogap in the optical conductivity is calculated based on the parameters in the model.

DOI: 10.1103/PhysRevB.66.075120 PACS number(s): 71.10.Fd, 71.30.+h, 75.10.Lp

The motivation for this work is the observation of a pseudogap that opens up in optical conductivity measurements of the three-dimensional transition metal oxide $SrRuO_3$[1] above its ferromagnetic transition temperature of $T_C \approx 150$ K. A pseudogap has also recently been seen in $BaRuO_3$.[2] In this pseudogapped regime, $\rho(T)$ increases linearly with temperature, passing through the Ioffe-Regel limit without saturation,[3] a behavior indicative of a ''bad metal.''[4] The optical conductivity in this state is proportional to the non-Fermi-liquid behavior of $\omega^{-1/2}$ at high frequency and has a peak at low frequencies[1] at approximately 250 cm^{-1}, the precise location of the peak being temperature dependent.

We propose that this pseudogap state can be understood by considering a ground state with spontaneously generated electronic currents circulating around the plaquettes. The currents arise from electron-electron correlations, due to the biquadratic terms in the Hamiltonian. The state that we propose is a generalization of the two-dimensional flux states invented by Affleck and Marston,[5] and studied in their chiral extension by Wen, Wilzcek, and Zee.[6] Unlike the two-dimensional case, there is no possibility of fractional statistics in three dimensions. However, the spontaneous generation of gauge fields is a possibility in three dimensions, and these gauge fields can lead to a ground state with circulating electronic currents. Earlier work was done on three-dimensional flux states by Libby and coworkers[7,8] and Zee.[9]

In actuality, $SrRuO_3$ has five bands crossing the Fermi surface formed by hybridizing the ruthenium d orbitals with the oxygen p orbitals.[10] The crystal structure is orthorhombic, becoming cubic at temperatures greater than 900 K.[11] Undoubtedly, the actual electronic structure of $SrRuO_3$, and particularly the presence of a van Hove singularity near the Fermi surface, influence the material's behavior. The model that we consider is vastly simplified and serves as a starting point for considering the nature of the pseudogapped state in the three-dimensional transition metal oxides. A model which incorporates some of these electronic features, but does not focus on the pseudogap regime, has been proposed by Laad and Müller-Hartmann.[12]

Based on the experimental evidence, it is clear that electron correlation effects are extremely important in understanding the physics of $SrRuO_3$. It has been suggested by Ahn *et al.*[13] that $SrRuO_3$ is near a Mott transition, and can be driven even closer to the transition by doping with calcium to form $Ca_xSr_{1-x}RuO_3$. Data from photoemission[14] and optical conductivity[13] experiments provide evidence that the on-site Coulomb repulsion is substantial in $SrRuO_3$, on the order of $U = 3-5$ eV, in spite of the extended nature of the $4d$ electron wavefunctions, and a value of 5 eV has been used by Laad and Müller-Hartmann.[12] The value of the hopping term can be obtained from the linearized argumented plane-wave calculations performed by Mazin *et al.*[10] The hopping element between the ruthenium orbitals is given by $V_{pd}^2/(\epsilon_d - \epsilon_p)$, where V_{pd} is the Ru-O overlap and the ϵ are the on-site energies. For the primarily t_{2g}-p_π band, this gives a hopping element of $t \approx 1$ eV.

I. MODEL SYSTEM

Given the proximity of $SrRuO_3$ to a Mott transition and the large value of the Coulomb repulsion, we believe that a consideration of the t-J model can give insight into the physics of $SrRuO_3$. The Hamiltonian that we consider is therefore the single orbital t-J model given by

$$H = J\sum_{\langle ij\rangle} \mathbf{S}_i \cdot \mathbf{S}_j - t\sum_{\langle ij\rangle\sigma} c_{i\sigma}^\dagger c_{j\sigma}, \tag{1}$$

where the sum over $\langle ij\rangle$ denotes nearest neighbors on a cubic three-dimensional lattice. Taking $J = 4t^2/U$ and using the values above gives a J corresponding to a Néel temperature of approximately 10^3 K. Implicit in this equation is that we have set $U = \infty$. The hopping matrix element t which appears in Eq. (1) is taken to be an effective hopping element, which has been greatly reduced due to this on-site Coulomb repulsion. The value of t will be set by two calculations in this paper: the stability of the flux phase versus other mean field states calculated in Sec. II, and the value of the optical conductivity calculated in Sec. V.

The spin operators may be written in terms of the fermion operators to give the Hamiltonian

$$H = -\frac{J}{2}\sum_{\langle ij\rangle}\sum_{\sigma\sigma'} c_{i\sigma}^\dagger c_{j\sigma} c_{j\sigma'}^\dagger c_{i\sigma'} - t\sum_{\langle ij\rangle}\sum_{\sigma} c_{i\sigma}^\dagger c_{j\sigma} + \frac{3\mathcal{N}J}{4}. \tag{2}$$

The Hamiltonian will be treated in the mean field, or Hartree-Fock, approximation. We make the replacement

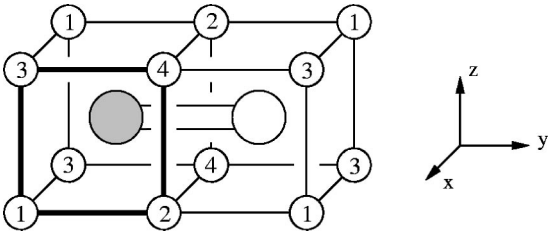

FIG. 1. Unit cell for the symmetry-broken bond Hamiltonian. The dark line passes through the four atoms in the planar unit cell. The spheres at the center of the cubes represent oppositely charged Dirac monopoles with the ''tail'' running through the interface between the two cubes.

$$\sum_{\sigma} c_{i\sigma}^{\dagger} c_{j\sigma} \rightarrow \chi_{ij} + \left(\sum_{\sigma} c_{i\sigma}^{\dagger} c_{j\sigma} - \chi_{ij} \right). \tag{3}$$

The assumption is made that the term in brackets, which corresponds to fluctuations about the mean field χ_{ij}, is small and can be included only to linear order. The resulting Hamiltonian is given by

$$H = \frac{J}{2} \sum_{\langle ij \rangle} \left\{ \left| \chi_{ij} \right|^2 - 2 \left[\left(\chi_{ij} + \frac{t}{J} \right) c_j^{\dagger} c_i + \text{H.c.} \right] \right\}, \tag{4}$$

where we have dropped the redundant spin index. There is no *a priori* reason to believe that the fluctuations about the mean field will be small, although it has been rigorously shown in the two-dimensional case for the large-n limit,[5] where n is the particle spin.

We allow the χ_{ij} to break the translational symmetry of the lattice. We choose a four-atom unit cell as shown in Fig. 1. The lattice is generated by the primitive translation vectors $(1,0,1)$, $(1,0,-1)$, and $(0,2,0)$, in units of the bond length b. The χ_{ij} in Eq. (4) are then parametrized by 12 complex numbers. We use the notation $\chi_{i\nu}$, where the index $i = 1, \ldots, 4$ is the location of the atom in the unit cell and the index ν gives the direction $\{x,y,z\}$.

This choice is made because it allows for the formation of a π per plaquette flux phase, something that a two atom unit cell does not allow in three dimensions. The model is computationally simpler than the eight-band model studied by Libby and co-workers,[7,8] at the expense of picking out a preferred direction. To get a feel for what this corresponds to, one can think of the gauge fields in the sample as being generated by Dirac monopoles of alternating charge sitting at the centers of each cube. The ''tails'' of the monopoles are connected to form dipoles. The $\hat{\boldsymbol{y}}$ direction in our model corresponds to the dipolar axis.

The self-consistency of the model is the requirement that the energy as determined by Eq. (4) be a local minimum with respect to variations of the 12 complex parameters $\chi_{i\nu}$. This can be seen by writing

$$\langle H \rangle = \frac{\mathcal{N}J}{8} \sum_{i=1}^{4} \sum_{\nu=1}^{3} \left\{ |\chi_{i\nu}|^2 - 2 \left[\left(\chi_{i\nu}^{*} + \frac{t}{J} \right) \langle c_i^{\dagger} c_{i+\nu} \rangle + \text{H.c.} \right] \right\}. \tag{5}$$

Minimizing this function with respect to $\chi_{i\nu}^{*}$ gives the self-consistency relation

$$\langle c_i^{\dagger} c_{i+\nu} \rangle = \frac{\chi_{i\nu}}{2}. \tag{6}$$

Also note that, at this minimum, the expectation value of the Hamiltonian is given by

$$\langle H \rangle = -\frac{\mathcal{N}J}{8} \sum_{i=1}^{4} \sum_{\nu=1}^{3} \left[|\chi_{i\nu}|^2 + 2\frac{t}{J} \text{Re}(\chi_{i\nu}) \right]. \tag{7}$$

The Hamiltonian in Eq. (4) contains both a field strength and a term which we define as the bond Hamiltonian:

$$H_B = J \sum_{\langle ij \rangle} \sum_{\sigma} \left(\chi_{ji} + \frac{t}{J} \right) c_{i\sigma}^{\dagger} c_{j\sigma} + \text{H.c.} \tag{8}$$

The bond Hamiltonian can be diagonalized by introducing a set of operators

$$\psi_{\mathbf{q}\lambda}^{\dagger} = \frac{1}{\sqrt{\mathcal{N}}} \sum_{l} e^{i\mathbf{q}\cdot\mathbf{r}_l} u_{\mathbf{q}\lambda}(l) c_{\mathbf{r}_l}^{\dagger}, \tag{9}$$

where $\mathcal{N}$ is the number of sites in the lattice, λ is the band index that runs from 1 to 4, and the $u_{\mathbf{q}\lambda}(l)$ are a set of functions periodic in the unit cell. The bands are determined by the eigenvalue equation

$$H_{\mathbf{q}} u_{\mathbf{q}\lambda} = \epsilon_{\mathbf{q}\lambda} u_{\mathbf{q}\lambda}, \tag{10}$$

where $H_{\mathbf{q}}$ is written in terms of the hopping elements and $u_{\mathbf{q}\lambda}$ is a four-component vector $u_{\mathbf{q}\lambda}(1) \cdots u_{\mathbf{q}\lambda}(4)$. For the unit cell depicted in Fig. 1, the Hamiltonian takes the form

$$H_{\mathbf{q}} = J \begin{pmatrix} 0 & \eta_1 & \eta_3 & 0 \\ \eta_1^{*} & 0 & 0 & \eta_4 \\ \eta_3^{*} & 0 & 0 & \eta_2 \\ 0 & \eta_4^{*} & \eta_2^{*} & 0 \end{pmatrix}, \tag{11}$$

where

$$\begin{aligned} \eta_1 &= \tilde{\chi}_{1y} e^{iq_y} + \tilde{\chi}_{2y}^{*} e^{-iq_y}, \\ \eta_2 &= \tilde{\chi}_{3y} e^{iq_y} + \tilde{\chi}_{4y}^{*} e^{-iq_y}, \\ \eta_3 &= \tilde{\chi}_{1x} e^{iq_x} + \tilde{\chi}_{1z} e^{iq_z} + \tilde{\chi}_{3x}^{*} e^{-iq_x} + \tilde{\chi}_{3z}^{*} e^{-iq_z}, \\ \eta_4 &= \tilde{\chi}_{2x} e^{iq_x} + \tilde{\chi}_{2z} e^{iq_z} + \tilde{\chi}_{4x}^{*} e^{-iq_x} + \tilde{\chi}_{4z}^{*} e^{-iq_z}. \end{aligned} \tag{12}$$

The tilde in the expression above means that these numbers include the actual hopping element: $\tilde{\chi}_{i\nu} = \chi_{i\nu} + t/J$. The eigenenergies for the four bands are given by

$$\epsilon_{\mathbf{q}} = \pm J \sqrt{\frac{\eta_i \eta_i^{*}}{2} \pm \sqrt{\left(\frac{\eta_i \eta_i^{*}}{2} \right)^2 - |\eta_1 \eta_2^{*} - \eta_3 \eta_4^{*}|^2}}, \tag{13}$$

with the usual Einstein summation convention. In Sec. III we will consider the band structure and eigenstates of one par-

ticular solution of the bond Hamiltonian, the flux state where the hopping elements are complex and equal in magnitude: $|\chi_{i\nu}|=\chi$ for all i,ν.

For $t=0$ the gauge fields χ_{ij} are unobservable. However, as soon as t is increased they lead to real circulating electronic currents. Consider the site i and the six sites j that are its nearest neighbors. The sum of the currents flowing outward from site i is then the time rate of change of the number operator n_i on site i,

$$\sum_j j_{ij}=\left\langle \frac{\partial}{\partial t}n_i \right\rangle = \frac{i}{\hbar}\langle [H_B,n_i]\rangle = \frac{2i}{\hbar}\sum_j (J\chi_{ij}+t)\langle c_j^\dagger c_i\rangle - \text{H.c.}, \tag{14}$$

where the factor of 2 arises from the spin. The term $\chi_{ij}\langle c_j^\dagger c_i\rangle$ is real and gives no contribution, but for $t>0$ and χ_{ij} complex, the bonds carry electronic currents. These currents are the signature of the flux state. They have long-range order and can be probed by neutron diffraction, as will be shown in Sec. IV.

II. THE PHASE DIAGRAM

The Hamiltonian described in Sec. I admits a number of self-consistent solutions. We have performed a numerical search as a function of the hopping element t and the doping δ. The function to be minimized is

$$E=\frac{\mathcal{N}}{8}\left[J\sum_{i\nu}|\chi_{i\nu}|^2+2\frac{1}{\mathcal{N}_m}{\sum_{\mathbf{k}\lambda}}' \epsilon_{\lambda\mathbf{k}}\right], \tag{15}$$

where $\mathcal{N}_m=\mathcal{N}/4$ is the number of unit cells in the lattice. The search is performed using Powell's method in the space of the $\chi_{i\nu}$. At each point in the space, the bands are determined by Eq. (13), and the lower magnetic bands are filled up with $N_e=\mathcal{N}(1-\delta)$ electrons.

Our search is limited to three classes of states. We consider the flux phase with $|\chi_i|=|\chi|$ for all i, with the phases of the hopping elements unconstrained. At $t=\delta=0$ the flux phase has a flux $\Phi=\pi$ per plaquette as defined by

$$e^{i\Phi}=\prod_{\text{plaquette}}\frac{\tilde{\chi}_{i\nu}}{|\tilde{\chi}_{i\nu}|}. \tag{16}$$

Note that a flux of π and a flux of $-\pi$ per plaquette are indistinguishable since in either case the electron acquires a phase of -1 upon traversing the plaquette. This is the chiral symmetry of the model. Away from $t=\delta=0$, the flux per plaquette is no longer π and the chiral symmetry is broken.

Another state that we have considered is the dimer state. In this case each site forms a bond with a neighboring site. In the case of $t=\delta=0$, one particular manifestation of the state is $\chi_{1z}=\chi_{4x}=1$ with all other $\chi_{i\nu}=0$. The dimer state has flat bands ($\epsilon_{\mathbf{q}}=\pm J$) and can be considered to be a charge-density state with the charge localized on the bonds for which $\chi_{i\nu}=1$.[5] Away from the point $t=\delta=0$, the state becomes partially dimerized. There are in principle a number of nonequivalent dimer solutions, but the solution mentioned above appears to be the lowest energy configuration.

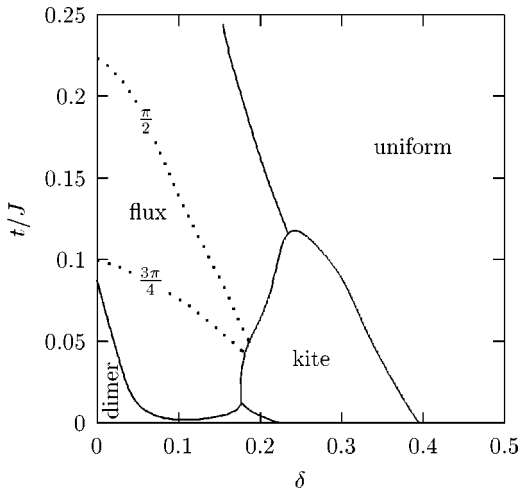

FIG. 2. Phase diagram for bond states. The diagram shows the competition between the four types of states considered in the text. The contours in the flux phase region show the average flux per plaquette, as defined by Eq. (16).

At values of $\delta\gtrsim 0.2$ another local minimum is the kite state which has $\chi_{1y}=\chi_{2x}=\chi_{3z}=\chi_{4y}\neq\chi_{i\nu}$. The state is called a kite state because the lines of charge, if the analogy from the dimer state above is used, form zigzagging patterns through the lattice, and could lead to a lattice distortion from the large Coulomb repulsion between charged lines. This particular instantiation of the kite state is chosen for the same reasons as the dimer above. The last state that is considered is the uniform state with all $\chi_{i\nu}$ equal and real valued. This state is a simple Fermi liquid, with a renormalized value of the hopping matrix element.

The phase diagram is shown in Fig. 2. While we have performed the calculation for an arbitrary flux state as described above, the phase diagram shows a calculation performed using a restricted parameter set. The parameters used are shown as different arrows in Fig. 3 below. This is done because at $\delta\approx 0.1$, there is a transition to a flux phase with a

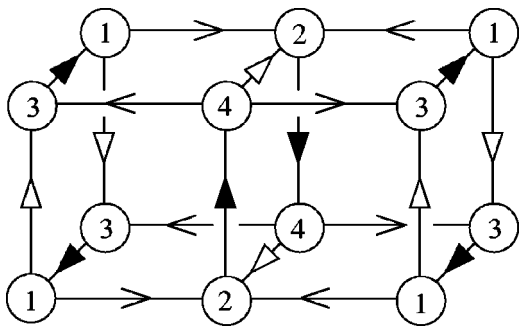

FIG. 3. The π per plaquette flux phase. All bonds have the same magnitude. The arrows correspond to complex phases of ϕ (>), $\phi-\pi/4$ (▷), and $3\pi/4-\phi$ (▶), where ϕ is determined by $\tan\phi=\sqrt{2}$. This diagram shows the same portion of the lattice as is shown in Fig. 1.

different type of ordering which is outside the scope of the current discussion. Apart from this transition, there is no qualitative change in the phase diagram when the unconstrained flux state is considered. From the phase diagram we see that the flux state is stabilized over a fairly wide range of doping, but that the flux per plaquette decreases from the value of π as one leaves the point $t=\delta=0$. In the calculations which follow we will assume that $t/J=0.1$, a point at which the highly symmetric π per plaquette flux state discussed below in Sec. III is a reasonable approximation to the actual mean field state.

One must also consider the possibilities of other types of order which are not described by the mean-field χ_{ij}. The most insidious of these is antiferromagnetic order. At $t=\delta=0$, the energies of the two stabilized states discussed above are

$$E_{\text{dimer}}=-\frac{\mathcal{N}J}{4}, \quad E_{\text{flux}}\approx -0.95\frac{\mathcal{N}J}{4}. \tag{17}$$

For comparison, the Néel state, which is characterized by

$$\chi_{ij}=0 \quad \langle c^{\dagger}_{i\sigma}\sigma^{z}c_{i\sigma'}\rangle=(-1)^{i}, \tag{18}$$

has an energy of $-3\mathcal{N}J/4$, lower than either of the two bond states at $t=\delta=0$. In order for the bond states to be actualized, a term has to be added which will destabilize the antiferromagnetic order. This can be done by adding a next-nearest-neighbor hopping term J',[15] in which case the energy of the Néel state will be

$$E_{\text{Néel}}=-\frac{3\mathcal{N}J}{4}\left(1-2\frac{J'}{J}\right). \tag{19}$$

The energies of the bond states are actually unchanged up to a value of $J'/J\approx 1/3$, which is the threshold for acquiring a nonzero value of the next-nearest neighbor χ_{ij} as shown by Laughlin and Zou.[16] At the value $J'=J/3$, the energy of the Néel state is equal to the energy of the dimer state and very close to the energy of the flux state. Doping will also serve to destabilize the antiferromagnet so that the crossover will actually occur at a lower value of J' than the one reported here. Therefore, while it is not treated explicitly in this paper, some term such as the next-nearest neighbor J' must be added to this model in order to make the bond states energetically favorable with respect to the Néel-ordered state.

III. FLUX PHASE

In the calculations which follow, we consider the π per plaquette flux phase described in Sec. II, which is only truly stabilized at $\delta=t=0$. Some care must be used in selecting this state, since at $t=\delta=0$ the system is invariant under a gauge transformation where

$$c_i\rightarrow e^{i\phi_i}c_i, \quad \chi_{ij}\rightarrow e^{i(\phi_j-\phi_i)}\chi_{ij}. \tag{20}$$

Away from this point, this symmetry disappears, and the low-energy state is the one for which the quantity

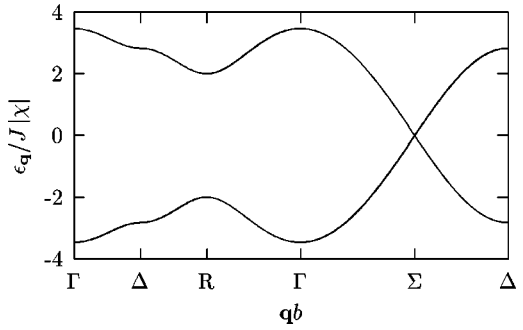

FIG. 4. Flux phase band structure. Points in the Brillouin zone are $\Gamma=(0,0,0)$, $\Delta=(\pi/2,0,0)$, $R=(\pi/2,0,\pi/2)$, and $\Sigma=(\pi/2,\pi/2,\pi/2)$. There are two distinct Dirac points located at $\mathbf{q}b=(\pi/2,\pi/2,\pi/2)$ and $\mathbf{q}b=(\pi/2,\pi/2,-\pi/2)$.

$$\sum_{i\nu}\text{Re}[\chi_{i\nu}], \tag{21}$$

is a maximum as can be seen from Eq. (7). The state is shown in Fig. 3. It can be found either by maximizing the function in Eq. (21) for an arbitrary gauge transformation, or by numerically continuing a state from $t>0$ down to $t=0$. The choice of the correct symmetry-breaking gauge is important since it will affect the distribution of electronic currents in the sample and hence observable features such as the neutron diffraction and optical conductivity.

In this state, the Hamiltonian in Eq. (9) can be rewritten using a set of Dirac matrices α_x, α_y, and α_z, such that

$$H_{\mathbf{q}}=2J|\chi|\sum_{\nu}\cos(q_\nu b)\alpha_\nu, \tag{22}$$

where the matrices satisfy the algebra

$$\{\alpha_i,\alpha_j\}=2\delta_{ij}. \tag{23}$$

Explicit forms for the matrices are given in the Appendix. It is found numerically that $|\chi|\approx 0.4$. The eigenvalues of the Hamiltonian are twofold degenerate and are given by

$$\epsilon_{\mathbf{q}}=\pm 2J|\chi|\sqrt{\sum_{\nu}\cos^2(q_\nu b)}. \tag{24}$$

The band structure is shown in Fig. 4. At half-filling the Fermi surface reduces to two isolated points at $\mathbf{q}b=(\pi/2,\pi/2,\pi/2)$ and $\mathbf{q}b=(\pi/2,\pi/2,-\pi/2)$ shown at the point Σ in Fig. 4. The low-energy excitations about these points are relativistic.

In order to calculate the neutron cross section and the optical conductivity, we also will need the eigenvectors which appear in Eq. (9). The matrix $\mathbf{u}$ whose rows correspond to the bands $1\ldots 4$ and whose columns correspond to the position in the unit cell is given by

$$\mathbf{u}_{\mathbf{q}}=\frac{1}{\sqrt{2}}\begin{pmatrix} |\eta_{\mathbf{q}}| & -\frac{\eta_{\mathbf{q}}}{|\eta_{\mathbf{q}}|}e^{-i\phi} & 0 & \gamma_{\mathbf{q}}\frac{\eta_{\mathbf{q}}}{|\eta_{\mathbf{q}}|} \\ |\gamma_{\mathbf{q}}| & 0 & \frac{\gamma_{\mathbf{q}}}{|\gamma_{\mathbf{q}}|}e^{-i\phi} & -\eta_{\mathbf{q}}\frac{\gamma_{\mathbf{q}}}{|\gamma_{\mathbf{q}}|} \\ |\eta_{\mathbf{q}}| & \frac{\eta_{\mathbf{q}}}{|\eta_{\mathbf{q}}|}e^{-i\phi} & 0 & -\gamma_{\mathbf{q}}\frac{\eta_{\mathbf{q}}}{|\eta_{\mathbf{q}}|} \\ |\gamma_{\mathbf{q}}| & 0 & -\frac{\gamma_{\mathbf{q}}}{|\gamma_{\mathbf{q}}|}e^{-i\phi} & -\eta_{\mathbf{q}}\frac{\gamma_{\mathbf{q}}}{|\gamma_{\mathbf{q}}|} \end{pmatrix}, \tag{25}$$

where we have defined the quantities

$$\eta_{\mathbf{q}}=\frac{\cos q_y b}{\Gamma_{\mathbf{q}}}, \quad \gamma_{\mathbf{q}}=e^{-i\pi/4}\frac{\cos q_x b - i\cos q_z b}{\Gamma_{\mathbf{q}}},$$

$$\Gamma_{\mathbf{q}}=\sqrt{\sum_{\nu}\cos^2(q_\nu b)}. \tag{26}$$

The phases of the eigenvectors in Eq. (25) have been selected so that the eigenstates in Eq. (9) are invariant under $\mathbf{q}\rightarrow\mathbf{q}+\mathbf{Q}$ where $\mathbf{Q}$ is any vector in the reciprocal lattice.

IV. NEUTRON SCATTERING

The flux states can be probed by neutron scattering, as the neutron spin interacts with the magnetic dipoles generated by the real electron currents circulating on the plaquettes. The interaction potential[17] is written

$$V(\mathbf{r})=2\sum_{\langle ij\rangle} t(c_i^\dagger c_j-\text{H.c.})\exp\left[\frac{ie}{\hbar c}\int_{\mathbf{x}_i}^{\mathbf{x}_j}\mathbf{A}\cdot dl\right], \tag{27}$$

where the vector potential is given by

$$\mathbf{A}=\boldsymbol{\mu}\times\frac{\mathbf{r}_e-\mathbf{r}_n}{|\mathbf{r}_e-\mathbf{r}_n|^3}, \quad \boldsymbol{\mu}=-\gamma\frac{e\hbar}{m_n c}\mathbf{S}. \tag{28}$$

In these expressions $\mathbf{S}$ is the neutron spin and $\gamma\approx 1.91$ is a constant. It can be shown[18] that

$$\int d\mathbf{r}e^{i\mathbf{q}\cdot\mathbf{r}_n}V(\mathbf{r})$$

$$=i(\gamma r_0)\left(\frac{m}{m^*}\right)\frac{8\pi\hbar^2}{m_n}\frac{1}{|\mathbf{q}b|^2}\sum_{\nu} J_\nu\frac{\hat{\boldsymbol{\nu}}\cdot(\mathbf{S}\times\mathbf{q})}{\mathbf{q}\cdot\hat{\boldsymbol{\nu}}}, \tag{29}$$

with the current operator defined as

$$J_\nu=\sum_{\mathbf{k}} c_{\mathbf{k}+\mathbf{q}}^\dagger c_{\mathbf{k}} f_\nu(\mathbf{k},\mathbf{q}),$$

$$f_\nu(\mathbf{k},\mathbf{q})=\cos(k_\nu b)-\cos(k_\nu b+q_\nu b). \tag{30}$$

In these expressions we have replaced the hopping element t by $\hbar^2/(2m^*b^2)$, with m^* the effective mass. Since we are assuming (see Sec. II) that $t/J=0.1$, the effective mass will be quite large. If we assume that J takes the typical value of 0.1 eV, we have $m^*\approx 15m$. The vector $\hat{\boldsymbol{\nu}}$ is a unit vector with the sum running over the x, y, and z directions.

Converting this to a cross section and averaging over the spin, assuming that the incoming beam is unpolarized, the expression for the cross section is given by

$$\frac{d\sigma}{d\Omega}=(\gamma r_0)^2\left(\frac{m}{m^*}\right)^2\frac{4}{|\mathbf{q}b|^4}\sum_{\nu<\nu'}\left|\frac{q_\nu}{q_{\nu'}}\langle J_{\nu'}\rangle-\frac{q_{\nu'}}{q_\nu}\langle J_\nu\rangle\right|^2. \tag{31}$$

In order to calculate the matrix elements in Eq. (31), we need to rewrite the current operator in terms of the eigenstates of our system. We first break up the momentum sum so that it runs only over the first Brillouin zone,

$$J_\nu=\sum_{\mathbf{k}}{}' \sum_{i=1}^{4} c_{\mathbf{k}+\mathbf{q}+\mathbf{Q}_i}^\dagger c_{\mathbf{k}+\mathbf{Q}_i} f_\nu(\mathbf{k}+\mathbf{Q}_i,\mathbf{q}), \tag{32}$$

where $\mathbf{Q}_1 b=\mathbf{0}$, $\mathbf{Q}_2 b=(\pi,0,\pi)$, $\mathbf{Q}_3 b=(0,\pi,0)$, and $\mathbf{Q}_4 b=\boldsymbol{\pi}$. We can rewrite the electron operators at momentum $\mathbf{k}+\mathbf{Q}$ in terms of the $c_{\mathbf{q}}(l)$ defined as

$$c_{\mathbf{q}}^\dagger(l)=\frac{1}{\sqrt{\mathcal{N}_m}}\sum_{\mathbf{R}} e^{i\mathbf{q}\cdot(\mathbf{R}+\mathbf{r}_l)}c_{\mathbf{R}+\mathbf{r}_l}^\dagger, \tag{33}$$

where $\mathbf{R}$ runs over all the unit cells and $\mathbf{r}_l$ is the position of the lth atom in the unit cell. This introduces a matrix g with elements $g_{il}=\exp[i\mathbf{Q}_i\cdot\mathbf{r}_l]/2$, and results in the current operator

$$J_\nu=\sum_{\mathbf{k}}{}' \sum_{imp} g_{im}g_{ip}c_{\mathbf{k}+\mathbf{q}}^\dagger(m)c_{\mathbf{k}}(p)f_\nu(\mathbf{k}+\mathbf{Q}_i,\mathbf{q}). \tag{34}$$

We also note that $f_\nu(\mathbf{k}+\mathbf{Q}_i,\mathbf{q})=[\bar{Q}^\nu]_{ii}f_\nu(\mathbf{k},\mathbf{q})$, where the matrix $\bar{Q}^\nu$ is diagonal with elements $\exp[i\mathbf{Q}_i\cdot\boldsymbol{\nu}b]$. The sum on i can then be performed to obtain

$$J_\nu=\sum_{\mathbf{k}}{}' \sum_{mp} c_{\mathbf{k}+\mathbf{q}}^\dagger(m)[g\bar{Q}^\nu g]_{mp}c_{\mathbf{k}}(p)f_\nu(\mathbf{k},\mathbf{q}). \tag{35}$$

The matrix $g\bar{Q}^{\nu}g$ in the above expression has a natural interpretation. It merely connects all sites in the lattice are connected by a hopping element in the $\boldsymbol{\nu}$ direction. It can be written in the form

$$g\bar{Q}^{\nu}g=\begin{pmatrix}\sigma^x & 0\\ 0 & \sigma^x\end{pmatrix}\delta_{\nu y}+\begin{pmatrix}0 & 1\\ 1 & 0\end{pmatrix}(\delta_{\nu x}+\delta_{\nu z}). \tag{36}$$

Finally, we can rewrite Eq. (35) by inverting the eigenvector matrix in Eq. (25). This gives

$$J_{\nu}=\sum_{\mathbf{k}}{}' \sum_{\lambda\lambda'}[u_{\mathbf{k}}(g\bar{Q}^{\nu}g)u^{\dagger}_{\mathbf{k}+\mathbf{q}}]_{\lambda'\lambda}f_{\nu}(\mathbf{k},\mathbf{q})\psi^{\dagger}_{\lambda,\mathbf{k}+\mathbf{q}}\psi_{\lambda',\mathbf{k}}. \tag{37}$$

If we assume that the lower bands are completely filled, we can then write a simple expression for the expectation values of these matrix elements:

$$\langle J_{\nu}\rangle=\sum_{\boldsymbol{\tau}}\sum_{\mathbf{k}}{}' \mathrm{Tr}'[u_{\mathbf{k}}(g\bar{Q}^{\nu}g)u^{\dagger}_{\mathbf{k}+\mathbf{q}}]f_{\nu}(\mathbf{k},\mathbf{q})\delta_{\mathbf{q}\boldsymbol{\tau}}. \tag{38}$$

The prime on the trace indicates that it runs only over the lower two bands, and the sum on $\boldsymbol{\tau}$ runs over all vectors in the reciprocal lattice.

Expression (38) is quite general, and can be used to calculate properties away from zero doping by restricting the sum on $\mathbf{k}$ such that $\mathbf{k}<\mathbf{k}_F$. Additionally, this equation assumes nothing about the actual structure of the eigenvector matrix $u_{\mathbf{k}}$. Specializing to the case of the flux state discussed in Sec. III, the trace for $\nu=y$ is

$$i\left(1-\frac{\gamma^*_{\mathbf{k}+\mathbf{q}}}{\gamma^*_{\mathbf{k}}}\right)\eta_{\mathbf{k}}\sin\phi. \tag{39}$$

Here we have used the fact that $\eta_{\mathbf{k}+\mathbf{q}}=-\eta_{\mathbf{k}}$, a condition enforced by the presence of f_y in Eq. (38). We see that the trace is zero unless $\gamma_{\mathbf{k}+\mathbf{q}}=-\gamma_{\mathbf{k}}$, which means that $\langle J_y\rangle$ vanishes unless $q_{\nu}b$ is an odd multiple of π for all ν. For the $\nu=x$ and $\nu=z$ cases, the traces are the same as can be seen from Eq. (36). They are given by

$$i\left(1-\frac{\eta_{\mathbf{k}+\mathbf{q}}}{\eta_{\mathbf{k}}}\right)\mathrm{Im}\,\gamma_{\mathbf{k}}\cos\phi-i\left(1+\frac{\eta_{\mathbf{k}+\mathbf{q}}}{\eta_{\mathbf{k}}}\right)\mathrm{Re}\,\gamma_{\mathbf{k}}\sin\phi, \tag{40}$$

where we have taken $\gamma_{\mathbf{k}+\mathbf{q}}=-\gamma_{\mathbf{k}}$ for the same reasons as above. This expression takes two different values depending on whether q_yb is an even or an odd multiple of π.

Scattering will only occur at the reciprocal-lattice vectors, as guaranteed by the delta function in Eq. (38). The reciprocal lattice is shown in Fig. 5. There is no magnetic scattering at the nuclear locations, since they occur at even multiples of π. There is additionally no scattering at the line centers $\mathbf{q}b=\pi\hat{\boldsymbol{y}}$, since all three matrix elements vanish at these points. Scattering does occur at both the face centers at $\mathbf{q}b=(\pi,0,\pi)$ and at the body center at $\mathbf{q}b=\boldsymbol{\pi}$. The former distinguishes the scattering from Bragg scattering from a cubic antiferromagnet. It is likely that the actual material would consist of domains containing all possible dipolar orientations, so that scattering would actually be observed at all the face centers.

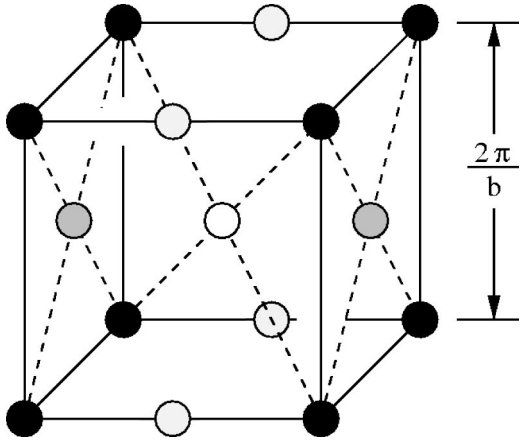

FIG. 5. Reciprocal-lattice vectors for the flux phase. The black dots show the scattering from the nuclear centers. The white dot shows the antiferromagnetic scattering vector at $\mathbf{q}b=\boldsymbol{\pi}$. The shaded dots at the face centers show those points in the reciprocal lattice space of the flux phase which produce scattering, and the lighter shaded dots along the line centers show those points in the reciprocal-lattice space which do not produce scattering.

The magnitude of the scattering will in general be quite small. We write the cross section as

$$\frac{d\sigma}{d\Omega}=\mathcal{N}_m\frac{(2\pi)^3}{v_{0m}}(\gamma r_0)^2\left(\frac{m}{m^*}\right)^2\sum_{\boldsymbol{\tau}}M(\mathbf{q})\delta(\mathbf{q}-\boldsymbol{\tau}), \tag{41}$$

where we have rewritten the Kronecker delta function from Eq. (38) in terms of the Dirac delta function with the proper normalization of $(2\pi)^3/V$. The term $v_{0m}=4b^3$ is the volume of the unit cell. The structure factor is given by

$$M(\mathbf{q})=\frac{4}{3}\frac{|\chi|^2}{|\mathbf{q}b|^2}\left[(3+\cos q_yb)\left(\frac{1}{(q_xb)^2}+\frac{1}{(q_zb)^2}\right)+4\frac{1-\cos q_yb}{(q_yb)^2}\right](1-\cos q_xb)(1-\cos q_zb). \tag{42}$$

In deriving this expression, we have repeatedly used the fact that

$$\frac{1}{\mathcal{N}_m}\sum_{\mathbf{k}}{}'\frac{\cos k_{\nu}\cos k_{\nu'}}{\Gamma_{\mathbf{k}}}=|\chi|\delta_{\nu\nu'}, \tag{43}$$

with the $\Gamma_{\mathbf{k}}$ defined as in Eq. (26). This relation follows from the symmetry of the momentum sum and Eq. (15). The structure factor in Eq. (42) takes the same value at the two smallest scattering angles corresponding to the points $\mathbf{Q}_2b=(\pi,0,\pi)$ and $\mathbf{Q}_4b=\boldsymbol{\pi}$ in the reciprocal lattice:

$$M(\mathbf{q})=\frac{64}{3\pi^4}|\chi|^2. \tag{44}$$

To give a feel for the order of magnitude of the scattering from the flux states, we compare to the scattering from an antiferromagnet. In that case one has

$$\frac{d\sigma}{d\Omega}|_{AF}=\frac{2}{3}\mathcal{N}_m^{AF}\frac{(2\pi)^3}{v_{0m}^{AF}}(\gamma r_0)^2\langle S^\eta\rangle^2\sum_{\boldsymbol{\tau}}|F(\boldsymbol{\tau})|^2\delta(\mathbf{q}-\boldsymbol{\tau}), \tag{45}$$

where the factor of 2/3 arises by assuming that the sublattice magnetization is along a crystallographic axis. We can estimate the form factor for the antiferromagnet by assuming it is the same as that of chromium, a typical band antiferromagnet. Chromium has a form factor of $F(\boldsymbol{\pi}/b)\approx 0.4$.[19] The unit cell in the flux phase is twice as large as the antiferromagnetic unit cell, and therefore $\mathcal{N}_m^{AF}=2\mathcal{N}_m$ and $v_{0m}^{AF}=v_{0m}/2$. Assuming that the spins are 50% polarized such that $\langle S^\eta\rangle=1/4$, and taking $m^*=15m$, we see that the scattering from the antiferromagnet is roughly 170 times larger than the scattering from the flux state at the wave vector $\mathbf{q}b=\boldsymbol{\pi}$. Note that the discrepancy in size is due primarily to the size of the effective hopping element t, which must be small compared to J if the flux phase is going to be stabilized away from $\delta=0$, as was shown in Sec. II.

V. OPTICAL CONDUCTIVITY

In our model, the peak in the optical conductivity arises from transitions between the bands shown in Fig. 4. The model is too simple to accurately predict the optical conductivity of a material such as $SrRu0_3$. However, the calculation illustrates both the dependence of the location of the peak on the spin-exchange energy J and the intensity of the peak on the ratio of t/J.

The calculation of the optical conductivity is very similar to that of the neutron diffraction. In this case we couple the system to a time-dependent vector potential $\mathbf{A}=A(t)\hat{\boldsymbol{\nu}}$, where the vector potential's time dependence and relation to the electric field are given by

$$A(t)=Ae^{-i\omega t},\quad \mathbf{E}=\frac{i\omega}{c}\mathbf{A}. \tag{46}$$

We assume that the wavelength of the light is long enough that we can ignore any spatial dependence in the fields. The vector potential couples to the hopping terms in the Hamiltonian. A phase is acquired according to

$$c_j^\dagger c_i\rightarrow c_j^\dagger c_i\exp\left[\frac{ie}{\hbar c}\int_{\mathbf{x}_i}^{\mathbf{x}_j}\mathbf{A}\cdot d\boldsymbol{l}\right]. \tag{47}$$

It is important to note that the corresponding χ_{ij} appearing in Eq. (4) also acquire an equal and opposite phase, so that when we expand the Hamiltonian to linear order in the vector potential $A(t)$ we do not get any contribution from the terms proportional to χ_{ij}. The perturbation to the Hamiltonian is

$$H'=-\frac{L}{c}\mathbf{A}\cdot\mathbf{j}, \tag{48}$$

where $L=\mathcal{N}^{1/3}b$ is the length of the sample and the current operator in the $\boldsymbol{\nu}$ direction is given by

$$j_\nu=\frac{2iteb}{\hbar L}\sum_i\left[c_i^\dagger c_{i+\boldsymbol{\nu}}-c_{i+\boldsymbol{\nu}}^\dagger c_i\right]. \tag{49}$$

Note that the operator in Eq. (49) defines the total current, not the current density, flowing in the $\boldsymbol{\nu}$ direction. The complex optical conductivity is related to the induced current density in the sample by

$$\mathbf{J}_{\rm ind}=\sigma\mathbf{E}. \tag{50}$$

The induced current can be calculated using linear response theory. In that case, it can be shown from Eqs. (46), (48), and (50) that the real portion of the optical conductivity is related to the complex portion of the current-current correlation function

$$\sigma_1(\omega)=-\frac{1}{\omega}\mathrm{Im}\chi(\omega), \tag{51}$$

where the current-current correlation function is given by

$$\chi(\omega)=\frac{1}{L}\sum_n|\langle 0|j|n\rangle|^2\left[\frac{1}{\hbar\omega-E_n+E_0+is}-\frac{1}{\hbar\omega+E_n-E_0+is}\right]. \tag{52}$$

The infinitesimal s arises from assuming that the perturbation in Eq. (48) vanishes at $t=-\infty$. The states $|0\rangle$ and $|n\rangle$ are to be evaluated at $t=-\infty$ or $\mathbf{A}=0$. The current operator in Eq. (49) can be written in terms of the eigenstates of the system, following the same approach applied in Eqs. (32)–(38). The result is that

$$j_\nu=4\frac{teb}{L\hbar}{\sum_{\mathbf{k}}}'\sum_{\lambda\lambda'}[u_{\mathbf{k}}(g\overline{Q}^\nu g)u_{\mathbf{k}}^\dagger]_{\lambda'\lambda}\sin(k_\nu b)\psi_{\lambda\mathbf{k}}^\dagger\psi_{\lambda'\mathbf{k}}. \tag{53}$$

Eq. (53) is very similar to Eq. (37). In this case, however, we are considering matrix elements connecting the ground state to excited states and so pick up the contributions at $\lambda\neq\lambda'$. Averaging the optical conductivity over the three directions in the lattice, it takes the form

$$\sigma_1(\omega)=\frac{\pi}{12|\chi|^2}\frac{e^2}{\hbar b}\left(\frac{t}{J}\right)^2\frac{1}{\mu}\frac{1}{\mathcal{N}_m}{\sum_{\mathbf{q}}}'F(\mathbf{q})\delta(\mu-\Gamma_{\mathbf{q}}), \tag{54}$$

where $\Gamma_{\mathbf{q}}$ was defined in Eq. (26) and where we have defined a dimensionless frequency given by $\mu=\hbar\omega/4J|\chi|$. The structure factor is given by

$$F(\mathbf{q})=\sum_\nu\sum_{\lambda=1}^{2}\sum_{\lambda'=3}^{4}|[u_{\mathbf{q}}(g\overline{Q}^\nu g)u_{\mathbf{q}}^\dagger]_{\lambda'\lambda}|^2\sin^2 q_\nu b. \tag{55}$$

The sums in Eq. (55) can be performed to give

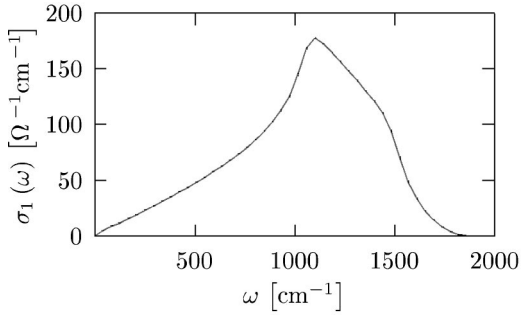

FIG. 6. Interband contribution to optical conductivity for the flux phase.

$$F(\mathbf{q})=\left(\frac{4}{3}+\frac{(\gamma_{\mathbf{k}}-\gamma_{\mathbf{k}}^{*})^2}{6}\right)(\sin^2 k_x b+\sin^2 k_z b)$$
$$+\frac{2}{3}(1+\eta_{\mathbf{k}}^2)\sin^2 k_y b, \tag{56}$$

with the quantities defined as in Eq. (26).

Equations (54) and (56) have been evaluated numerically, and the result is shown in Fig. 6. Within our model, the location of the peak is proportional to the exchange energy J. Assuming this takes the value 0.1 eV, we find that the peak occurs at approximately 1000 cm^{-1}, which gives order of magnitude agreement with the observed value of 250 cm^{-1} in $SrRuO_3$.[1] Due to the simplicity of the model we are solving, one would not expect more accurate agreement. The magnitude of the peak is governed by the ratio of t/J. A direct comparison of this quantity with experiment is more difficult. This is due to the fact that $SrRuO_3$ has five bands, whereas we have considered only a single orbital. Additionally, our calculation only considers the interband contribution to the conductivity, whereas the real material also has an intraband contribution from thermally excited carriers. If one assumes that the result shown in Fig. 6 needs to be scaled by a factor of roughly five to account for the number of orbitals in $SrRuO_3$, the results are reasonable compared with the measured conductivity of 6000 $\Omega^{-1}\,\mathrm{cm}^{-1}$.

VI. DISCUSSION

We propose that the three-dimensional flux state is a good candidate for the pseudogap state seen in the transition metal oxides. Its signature will be the presence of weak neutron-diffraction peaks arising from the ordered electronic currents in the material. The fact that $SrRuO_3$ is not near an antiferromagnetic transition and the fact that the three-dimensional flux states produce scattering at wave vectors other than $\mathbf{q}b=\boldsymbol{\pi}$ make the system an excellent candidate in which to observe this type of order. Further theoretical work is warranted to understand how the actual electronic structure of the material will influence the behaviors discussed here.

ACKNOWLEDGMENTS

We would like to thank R. Krishna and J. Franklin for many useful discussions, and S. Kivelson for inspirational remarks. We acknowledge support from the DOE through the Complex Materials Program at SSRL.

APPENDIX

The matrices from Eqs. (22) and (23) are given explicitly by

$$\alpha_x=\begin{pmatrix} 0 & 0 & Ze^{-3i\pi/4} & 0 \\ 0 & 0 & 0 & Z^{*}e^{i\pi/4} \\ Z^{*}e^{3i\pi/4} & 0 & 0 & 0 \\ 0 & Ze^{-i\pi/4} & 0 & 0 \end{pmatrix},$$

$$\alpha_z=\begin{pmatrix} 0 & 0 & Ze^{-i\pi/4} & 0 \\ 0 & 0 & 0 & Z^{*}e^{3i\pi/4} \\ Z^{*}e^{i\pi/4} & 0 & 0 & 0 \\ 0 & Ze^{-3i\pi/4} & 0 & 0 \end{pmatrix}, \tag{A1}$$

$$\alpha_y=\begin{pmatrix} 0 & Z & 0 & 0 \\ Z^{*} & 0 & 0 & 0 \\ 0 & 0 & 0 & Z^{*} \\ 0 & 0 & Z & 0 \end{pmatrix},$$

where

$$Z=e^{i\phi}=\frac{1}{\sqrt{3}}+i\sqrt{\frac{2}{3}}. \tag{A2}$$

*Electronic address: dfs@Stanford.edu

[1] P. Kostic, Y. Okada, N.C. Collins, Z. Schlesinger, J.W. Reiner, L. Klein, A. Kapitulnik, T.H. Geballe, and M.R. Beasley, Phys. Rev. Lett. **81**, 2498 (1998).
[2] Y.S. Lee, J.S. Lee, K.W. Kim, T.W. Noh, J. Yu, E.J. Choi, G. Cao, and J.E. Crow, Europhys. Lett. **55**, 280 (2001).
[3] L. Klein, J.S. Dodge, C.H. Ahn, J.W. Reiner, L. Mieville, T.H. Geballe, M.R. Beasley, and A. Kapitulnik, J. Phys.: Condens. Matter **8**, 10 111 (1996).
[4] V.J. Emery and S.A. Kivelson, Phys. Rev. Lett. **74**, 3253 (1995).
[5] I. Affleck and J.B. Marston, Phys. Rev. B **37**, 3774 (1988).
[6] X.G. Wen, F. Wilczek, and A. Zee, Phys. Rev. B **39**, 11 413 (1989).
[7] S.B. Libby, Z. Zou, and R.B. Laughlin, Nucl. Phys. B **348**, 693 (1991).
[8] A. Tikofsky, S.B. Libby, and R.B. Laughlin, Nucl. Phys. B **413**, 579 (1994).
[9] A. Zee, Int. J. Mod. Phys. B **5**, 529 (1991).
[10] I.I. Mazin, D.A. Papaconstantopoulos, and D.J. Singh, Phys. Rev. B **61**, 5223 (2000).

[11] B.C. Chakoumakos, S.E. Nagler, S.T. Misture, and H.M. Christen, Physica B **241-243**, 358 (1997).
[12] M.S. Laad and E. Müller-Hartmann, Phys. Rev. Lett. **87**, 246402 (2001).
[13] J.S. Ahn, J. Bak, H.S. Choi, T.W. Noh, J.E. Han, Y. Bang, J.H. Cho, and Q.X. Jia, Phys. Rev. Lett. **82**, 5321 (1999).
[14] K. Fujioka, J. Okamoto, T. Mizokawa, A. Fujimori, I. Hase, M. Abbate, H.J. Lin, C.T. Chen, Y. Takeda, and M. Takano, Phys. Rev. B **56**, 6380 (1997).
[15] M. Inui, S. Doniach, and M. Gabay, Phys. Rev. B **38**, 6631 (1988).
[16] R.B. Laughlin and Z. Zou, Phys. Rev. B **41**, 664 (1989).
[17] T.C. Hsu, J.B. Marston, and I. Affleck, Phys. Rev. B **43**, 2866 (1991).
[18] The reasoning leading to this result is identical to that of Affleck, Hsu, and Marston for the two-dimensional flux states (Ref. 17).
[19] E. Fawcett, Rev. Mod. Phys. **60**, 209 (1988).